CONFORMAL MAPPING VIA A DENSITY CORRESPONDENCE FOR THE DOUBLE-LAYER POTENTIAL

MATT WALA* AND ANDREAS KLÖCKNER*

Abstract. We derive a representation formula for harmonic polynomials and Laurent polynomials in terms of densities of the double-layer potential on bounded piecewise smooth and simply connected domains. From this result, we obtain a method for the numerical computation of conformal maps that applies to both exterior and interior regions. We present analysis and numerical experiments supporting the accuracy and broad applicability of the method.

Key words. conformal map, integral equations, Faber polynomial, high-order methods

AMS subject classifications. 65E05, 30C30, 65R20

1. Introduction. This paper presents an integral equation method for numerical conformal mapping, using an integral equation based on the *Faber polynomials* (on the interior) and their counterpart, *Faber-Laurent polynomials* (on the exterior). Our method is applicable to computing the conformal map from the interior and exterior of domains bounded by a piecewise smooth Jordan curve Γ onto the interior/exterior of the unit disk. Like most techniques for conformal mapping, this method relies on computing a boundary correspondence function between Γ and the boundary of the target domain. From the boundary correspondence, the mapping function can be derived via a Cauchy integral [25, p. 381].

The numerical construction of a function that maps the exterior of a simply connected region conformally onto the exterior of some other region arises in a number of applications including fluid mechanics [8, Ch. 4.5], the generation of finite element meshes for problems in fracture mechanics [45], the design of optical media [31], the analysis of iterative methods [15, 16, 40], and the solution of initial value problems [32]. The exterior mapping function's close relation to the Faber polynomials [11, 41] enables a number of the latter applications. Complex analytic functions defined inside a Jordan domain admit a near-optimal polynomial expansion in a basis of Faber polynomials [11, 19, 41]. By means of the *Faber transform*, this can be exploited numerically to perform polynomial or rational approximation [18]. A key step of this approximation procedure is the evaluation of the Faber polynomials themselves, which, given a numerically derived exterior boundary correspondence, can be achieved with an FFT-based method [17] or by applying Lemma 3.1 in this paper.

As a technical tool, we introduce a representation formula of complex-valued harmonic polynomials and Laurent polynomials in terms of the double-layer potential. The double-layer potential with a complex-valued density σ is given by

$$\mathcal{D}\sigma(x) = -\frac{1}{2\pi}\int_\Gamma \sigma(y)\,\hat{n}\cdot\nabla_y \log|y-x|\,ds(y), \quad x\notin\Gamma.$$

We study the density functions σ that give rise to polynomials on the *interior* in terms of the *exterior* Riemann map f^+. Specifically, in this paper, we prove that the images of the mth powers of the values of the exterior map $(f^+)^m$ used as a density under $\mathcal{D}$ are scaled Faber polynomials of degree m. Since the Faber polynomials form a basis for all complex polynomials, this result characterizes all densities that give rise

*Department of Computer Science, University of Illinois at Urbana-Champaign, 201 N. Goodwin Ave, Urbana, IL 61801 (wala1@illinois.edu, andreask@illinois.edu).

to polynomials under the double-layer operator. On the exterior domain, we study the representation of complex Laurent polynomials. We find, analogously to the interior case, that the images of the mth powers of values of the interior map $(f^-)^m$ under $\mathcal{D}$ are scaled Faber-Laurent polynomials on the exterior domain, where f^- is the interior mapping function. In both the polynomial and the Laurent polynomial case, letting $m = 1$ leads to a uniquely solvable integral equation from which the boundary correspondence of the interior or exterior map may be recovered by the solution of an integral equation identical to that of an appropriate Dirichlet problem of the Laplace equation.

Furthermore, we demonstrate how a Nyström discretization [34] using high-order accurate quadrature rules achieves high-order accuracy in the computed density. Our method is of practical interest because of the ready availability of fast solvers for second kind equations involving the double-layer potential. In the numerical examples of this paper we use an accelerated solver consisting of GMRES [38] with the required matrix-vector product driven by the Fast Multipole Method [9]. Since the number of GMRES iterations in our scheme does not depend on the mesh resolution, this solution scheme has an overall complexity of $O(n \log n)$, where n is the number of discretization points on the boundary.

Compared with the second-kind integral equation formulations in the existing literature, our method is perhaps operationally the most similar to Lichtenstein's method [4, 48], which is also based on the double-layer (Neumann) kernel, and methods based on the Kerzman-Stein kernel [28, 33]. Like our method, these methods are based on an integral equation whose solution is an easily invertible function of the boundary correspondence, and they can be used for both interior and exterior mapping. Similarly, these integral equation methods are also suitable for the Nyström method with trapezoidal rule. Nevertheless, our method differs from these because it is the only one which we are aware to make use that the images of powers of the Riemann map under the double-layer operator are Faber/Faber-Laurent polynomials.

Other integral equation formulations (e.g. due to Berrut [3], Warschawski [3], or Banin [25]) produce the derivative of the boundary correspondence, from which the boundary correspondence may be recovered by numerical integration. The integral equations of Gershgorin [25] and Kantorovich-Krylov [25, 27] may be used to recover the boundary correspondence directly, but since the solution is not periodic, this requires somewhat careful numerical treatment. Perhaps the most well-known first-kind equation is Symm's equation, which has been applied to the computation of both interior and exterior mapping functions [42, 43].

For methods for the reverse problem, that is, finding a conformal map from the interior/exterior of the unit disk onto the interior/exterior of a given domain, see, for instance [12, 13, 24]. For a comprehensive overview of methods for interior and exterior mapping, including methods not based on linear boundary integral equations, see Wegmann [48], Gaier [22], or Henrici [25]. The use of iterative methods and acceleration techniques also has a long history in the the solution of systems of equations arising in conformal mapping; see [35, 44, 47] for examples.

The remainder of this paper is organized as follows: In Section 2.1, we recall some facts about harmonic functions defined on interior or exterior domains, in particular relating to potential theory and the Cauchy integral, and in Section 2.2, we discuss the Faber and Faber-Laurent polynomials. Based on these preliminaries, we introduce our main technical results regarding the representation of harmonic polynomials and Laurent polynomials by double-layer potentials in Section 3. This allows us to develop a method for interior and exterior conformal mapping and a high-order discretization

method thereof, in Sections 4 and 5. We close with some numerical experiments on smooth and non-smooth domains in Section 6.

2. Preliminaries. In this paper, we work with a simple, closed, positively oriented curve Γ, which we assume to be piecewise smooth. The following conventions will be in use throughout the paper.

We will refer to the inner component of the curve Γ as Ω^- and to the outer component as Ω^+. Without loss of generality, we will assume $0 \in \Omega^-$.

We will use C_R to denote the set $\{z : |z| = R\}$.

The interior Riemann map f^- denotes the complex analytic bijection that maps Ω^- onto $\{z : |z| < 1\}$ such that $f^-(0) = 0$ and $(f^-)'(0)$ is a positive real number, ensuring uniqueness.

Similarly, we define the exterior Riemann map f^+ as the complex analytic bijection that maps Ω^+ onto $\{z : |z| > 1\}$ for which $\lim_{z\to\infty} f^+(z) = \infty$ and $\lim_{z\to\infty} (f^+)'(z)$ is a positive real number, again ensuring uniqueness.

Carathéodory's theorem [36] implies that the interior and exterior Riemann map continuously extend to the boundary Γ, establishing a one-to-one correspondence between Γ and the unit circle C_1. By the *boundary correspondences* we will mean the real multi-valued mappings θ^- and θ^+, defined on Γ, such that $\theta^\pm(w) = \arg f^\pm(w)$.

2.1. The Double-Layer Potential. The double-layer potential integral operator with density function $\varphi : \Gamma \to \mathbb{C}$ gives rise to a harmonic function f on the complement of Γ

$$f(x) = \mathcal{D}\varphi(x) = -\frac{1}{2\pi}\int_\Gamma \varphi(y)\, \hat{n}\cdot\nabla_y \log|y-x|\, ds(y), \quad x \in \mathbb{C}\setminus\Gamma. \tag{2.1}$$

Here $\hat{n}\cdot\nabla_y$ denotes the derivative with respect to the variable y along the outward-facing unit normal $\hat{n}$ at y. Where the normal is not defined or discontinuous, such as at a corner point, the kernel has a discontinuity.

Since $x \notin \Gamma$, in a neighborhood of y the value $|y-x|$ is nonzero and so the logarithm locally possesses a complex analytic branch. The Cauchy-Riemann equations then imply the relationship

$$\hat{n}\cdot\nabla_y \log|y-x| = \operatorname{Re}\hat{n}\cdot\nabla_y \log(y-x) = \operatorname{Im}\hat{\tau}\cdot\nabla_y \log(y-x)$$

between the normal derivative and the derivative with respect to the unit tangential vector to the curve, $\hat{\tau}$. Since

$$\hat{\tau}\cdot\nabla_y(\log(y-x)) = \lim_{h\to 0}\frac{1}{h}\left[\log(y-x+h\hat{\tau}) - \log(y-x)\right] = \frac{\hat{\tau}(y)}{y-x},$$

it follows that the double-layer potential $\mathcal{D}\sigma$ can be written as

$$f(x) = \mathcal{D}\sigma(x) = -\frac{1}{2\pi}\int_\Gamma \sigma(y)\left(\operatorname{Im}\frac{\hat{\tau}(y)}{y-x}\right) ds(y). \tag{2.2}$$

The kernel appearing in (2.2) is also referred to the *Neumann kernel* [25, Def. 15.9-4].

The equality (2.2) establishes a relationship between the double-layer potential and the Cauchy integral operator. Since $\hat{\tau}(y)ds(y) = dy$ and $\operatorname{Re} i\alpha = -\operatorname{Im}\alpha$, we have

$$f(x) = -\frac{1}{2\pi i}\int_\Gamma \sigma(y)\left(\operatorname{Re}\frac{1}{y-x}\right) dy, \tag{2.3}$$

and thus the kernel of the double-layer potential coincides with the real part of the Cauchy kernel [30, eqn. (7.37)].

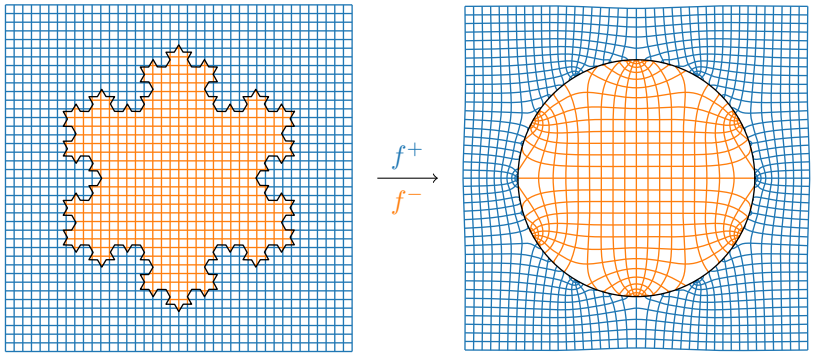

FIG. 2.1. *Graphical representation of the Riemann maps for the interior/exterior of a Koch snowflake with 192 corners.*

2.2. Faber Polynomials and Faber-Laurent Polynomials. Let $R > 0$ be sufficiently large that the domain Ω^- is contained within a disk of radius R centered at 0. Then, as f^+ is one-to-one for $|z| > R$, it follows that $g^+(w) := f^+(1/w)$ is one-to-one for $0 < |w| < 1/R$. The pole of g^+ at $w = 0$ is simple: Consider the root of $1/g^+$ at the origin. If it were a root of multiplicity m greater than one, then there would exist an $\epsilon \in \mathbb{C}$ so that the equation $1/g^+ = \epsilon$ has m simple roots [10, Thm. 7.4], in contradiction to g^+ being one-to-one. As a result, g^+ has the Laurent expansion

$$g^+(w) = f^+\left(\frac{1}{w}\right) = \frac{\alpha_1}{w} + \alpha_0 + \alpha_{-1}w + \alpha_{-2}w^2 + \cdots, \quad 0 < |w| < 1/R.$$

This implies that f^+ has the series representation

$$f^+(z) = \alpha_1 z + \alpha_0 + \frac{\alpha_{-1}}{z} + \frac{\alpha_{-2}}{z^2} + \cdots, \quad |z| > R. \tag{2.4}$$

The mth *Faber polynomial* $p_m(z)$ is defined as the terms of nonnegative power in the series for $f^+(z)^m$. It is a polynomial of degree m. Accordingly, $f^+(z)^m$ may be written as

$$f^+(z)^m = p_m(z) + \hat{p}_m(z) \tag{2.5}$$

where $\hat{p}_m(z)$ is a decaying (as $z \to \infty$) function of z defined on Ω^+.

The mth Faber-Laurent polynomial is defined in a similar manner using the function the $g^-(w) := 1/f^-(w)$ mapping Ω^- onto the exterior of the unit disk. This function, being injective on Ω^-, has a pole of order 1 at $w = 0$, and so for small enough $r > 0$ admits the Laurent expansion

$$g^-(w) = \frac{1}{f^-(w)} = \frac{\beta_{-1}}{w} + \beta_0 + \beta_1 w + \beta_2 w^2 + \cdots, \quad 0 < |w| < r.$$

The mth *Faber-Laurent polynomial* q_m is defined as the terms of negative power in the Laurent series for $g^-(w)^m$. We have the representation

$$g^-(w)^m = q_m(z) + \hat{q}_m(z),$$

where $\hat{q}_m(z)$ is a complex analytic function and $q_m(z)$ has a single order-m pole at 0.

3. Representation of Harmonic Polynomials and Laurent Polynomials.

LEMMA 3.1. *Let $m > 0$ be an integer. For all $z \in \Omega^-$, the mth Faber polynomial p_m satisfies*

$$p_m(z) = \frac{1}{\pi} \int_\Gamma f^+(y)^m \, \hat{n} \cdot \nabla_y \log|y - z| \, ds(y). \tag{3.1}$$

Effectively, the lemma states that the double-layer potential 'filters out' the decaying part of (2.5).

Proof. Let $z \in \Omega^-$. Denote the by $I(z)$ the integral

$$I(z) = \frac{1}{\pi} \int_\Gamma \operatorname{Re}\left(f^+(y)^m\right) \, \hat{n} \cdot \nabla_y \log|y - z| \, ds(y).$$

We provide a proof that $I(z) = \operatorname{Re} p_m(z)$, thus handling the case of the real part of p_m. The argument for the imaginary part of p_m is completely analogous to the one for the real part.

Because $|f^+(y)| = 1$ for $y \in \Gamma$, we can can write $\operatorname{Re}\left(f^+(y)^m\right)$ as

$$\operatorname{Re}\left(f^+(y)^m\right) = \frac{1}{2}\left(f^+(y)^m + \frac{1}{f^+(y)^m}\right).$$

Using this identity and the identification of the double-layer kernel with the real part of the Cauchy kernel (2.3), we can represent $I(z)$ as

$$I(z) = \operatorname{Re} \frac{1}{2\pi i} \int_\Gamma \left(f^+(y)^m + \frac{1}{f^+(y)^m}\right) \frac{1}{y - z} \, dy. \tag{3.2}$$

We proceed by breaking the integral on the right hand side of (3.2) into parts. We show

$$\frac{1}{2\pi i} \int_\Gamma \frac{f^+(y)^m}{y - z} \, dy = p_m(z). \tag{3.3}$$

We write

$$f^+(y)^m = p_m(y) + \hat{p}_m(y)$$

where $\hat{p}_m(y)$ goes to 0 as $|y| \to \infty$. From the Cauchy integral formula, we have

$$\frac{1}{2\pi i} \int_\Gamma \frac{p_m(y)}{y - z} \, dy = p_m(z).$$

To handle $\hat{p}_m$, let $R > 0$ be sufficiently large so that Ω is contained in the interior of the disk with boundary C_R. In Ω^+, the function $y \mapsto \hat{p}_m(y)/(y - z)$ is analytic (recall $z \in \Omega^-$). It follows from Cauchy's theorem that

$$\frac{1}{2\pi i} \int_\Gamma \frac{\hat{p}_m(y)}{y - z} \, dy = \frac{1}{2\pi i} \int_{C_R} \frac{\hat{p}_m(y)}{y - z} \, dy$$

Let $R \to \infty$. Since $\hat{p}_m(y) = O(|y|^{-1})$, the integrand in the previous equation is $O(|y|^{-2})$. It follows from a standard integral estimate that

$$\lim_{R \to \infty} \left| \frac{1}{2\pi i} \int_{C_R} \frac{\hat{p}_m(y)}{y - z} \, dy \right| = 0,$$

and thus

$$\frac{1}{2\pi i}\int_\Gamma \frac{\hat{p}_m(y)}{y-z}\,dy = 0.$$

This demonstrates (3.3) since

$$\frac{1}{2\pi i}\int_\Gamma \frac{f^+(y)^m}{y-z}\,dy = \frac{1}{2\pi i}\int_\Gamma \frac{p_m(y)+\hat{p}_m(y)}{y-z}\,dy = p_m(z).$$

Next, we show that

$$\frac{1}{2\pi i}\int_\Gamma \frac{1}{f^+(y)^m(y-z)}\,dy = 0. \tag{3.4}$$

Again, recall $z \in \Omega^-$. As in the previous paragraph, the integrand is an analytic function of y in Ω^+, so we can choose $R > 0$ sufficiently large so that by Cauchy's theorem

$$\frac{1}{2\pi i}\int_\Gamma \frac{1}{f^+(y)^m(y-z)}\,dy = \frac{1}{2\pi i}\int_{C_R} \frac{1}{f^+(y)^m(y-z)}\,dy.$$

Since $f^+(y)^m = \Theta(|y|^m)$, it follows that the integrand in the previous equation is $\Theta(|y|^{-(m+1)})$. By a standard integral estimate, we obtain that

$$\lim_{R\to\infty}\left|\frac{1}{2\pi i}\int_{C_R} \frac{1}{f^+(y)^m(y-z)}\,dy\right| = 0$$

which implies (3.4).

By adding together the right hand sides of (3.3) and (3.4) and then taking the real part, we obtain that $I(z) = \operatorname{Re} p_m(z)$ via (3.2). ∎

LEMMA 3.2. *Let $m > 0$ be an integer. For all $z \in \Omega^+$, the mth Faber-Laurent polynomial q_m satisfies*

$$\overline{q_m(z)} = -\frac{1}{\pi}\int_\Gamma f^-(y)^m\,\hat{n}\cdot\nabla_y \log|y-z|\,ds(y). \tag{3.5}$$

The overline notation $\overline{\cdot}$ denotes the complex conjugate.

Proof. Let $z \in \Omega^+$ and

$$I(z) = -\frac{1}{\pi}\int_\Gamma \operatorname{Re}\left(f^-(y)^m\right)\,\hat{n}\cdot\nabla_y \log|y-z|\,ds(y).$$

As in the proof of Lemma 3.1, we show that $I(z) = \operatorname{Re} q_m(z)$, and remark that the imaginary part of q_m can be handled similarly.

We start by representing $I(z)$ as

$$I(z) = -\operatorname{Re}\frac{1}{2\pi i}\int_\Gamma \left(f^-(y)^m + \frac{1}{f^-(y)^m}\right)\frac{1}{y-z}\,dy.$$

By Cauchy's theorem, it follows that

$$-\frac{1}{2\pi i}\int_\Gamma \frac{f^-(y)^m}{y-z}\,dy = 0. \tag{3.6}$$

We show that

$$q_m(z) = -\frac{1}{2\pi i}\int_\Gamma \frac{1}{f^-(y)^m(y-z)}\,dy. \tag{3.7}$$

We proceed by breaking up $1/f^-(y)^m$ into

$$\frac{1}{f^-(y)^m} = q_m(y) + \hat{q}_m(y)$$

where q_m is the mth Faber-Laurent polynomial, and $\hat{q}_m$ is the complex analytic part. First, we handle q_m. For y close to 0, we express

$$\frac{1}{y-z} = -\sum_{k=0}^{\infty} \frac{y^k}{z^{k+1}}, \qquad \text{and} \qquad q_m(y) = \sum_{k=1}^{m} \frac{a_k}{y^k}$$

for some (a_k). Multiplying both sums, collecting terms, and using the fact that q_m has a exactly one pole of order m at 0, we conclude that

$$\operatorname*{Res}_{y=0} \left(-q_m(y) \sum_{k=0}^{\infty} \frac{y^k}{z^{k+1}} \right) = -q_m(z),$$

which implies by the residue theorem that

$$-\frac{1}{2\pi i} \int_\Gamma \frac{q_m(y)}{y-z}\, dy = q_m(z).$$

Since $\hat{q}_m$ is an analytic function inside Ω^-, we have from Cauchy's theorem that

$$-\frac{1}{2\pi i} \int_\Gamma \frac{\hat{q}_m(y)}{y-z}\, dy = 0.$$

This demonstrates (3.7).

The result $I(z) = \operatorname{Re} q_m(z)$ follows by adding together (3.6) and (3.7) and then taking the real part. ∎

We briefly point out three related results in the literature. The basis (3.1) can also be derived from [25, Lemma 18.2d, p. 524], although our proof does not rely on this lemma. Gaier proves a result similar to the case $m = 1$ of Lemma 3.1, in [22, p. 14, (2.20)], for the case of a horizontal slit. Finally, in [33, (3.12)] a related integral equation is derived involving the derivative $(f^+)'$ and the adjoint Neumann kernel.

4. Integral Equations for Interior and Exterior Conformal Mapping. In this section, we develop a method for recovering the boundary correspondence assuming that the boundary Γ is smooth.

4.1. Exterior Case. This section derives an integral equation method for computing the boundary correspondence $\theta^+(z)$ for the exterior map f^+. We solve an integral equation corresponding to an interior Laplace Dirichlet problem to obtain a density function σ, and recover the boundary correspondence from the density by an application of the Cauchy integral formula and a normalization.

Recall the power series expansion of the exterior map

$$f^+(z) = \alpha_1 z + \alpha_0 + \frac{\alpha_{-1}}{z} + \frac{\alpha_{-2}}{z^2} + \cdots.$$

From Lemma 3.1 for $m = 1$, we have that for all $z \in \Omega^-$

$$\alpha_1 z + \alpha_0 = \frac{1}{\pi} \int_\Gamma f^+(y)\, \hat{n} \cdot \nabla_y \log|y-z|\, ds(y) = -2\mathcal{D} f^+(z).$$

Letting z approach a boundary point $\zeta \in \Gamma$ from the interior we obtain, using the inner jump relation for the double-layer potential [30, Thm. (6.18)], the integral equation

$$\alpha_1 \zeta + \alpha_0 = -2\mathcal{D} f^+(\zeta) + f^+(\zeta), \quad \zeta \in \Gamma.$$

The parameters α_1 and α_0 are not assumed to be known a priori. We use the fact that $\mathcal{D}$ is linear, and that for the constant density $1(\zeta)$, $\mathcal{D}1(\zeta) = -1/2$ [30, Ex. 6.17]. Using these two facts, let us define the density σ as

$$\sigma(\zeta) = -\frac{1}{\alpha_1}\left(2f^+(\zeta) - \alpha_0\right), \quad \zeta \in \Gamma.$$

Then we can write the previous integral equation as

$$\zeta = \left(\mathcal{D} - \frac{1}{2}\right)\sigma(\zeta), \quad \zeta \in \Gamma. \tag{4.1}$$

This integral equation is uniquely solvable [30, Thm. 6.21]. From the density σ, we can recover f^+ and the boundary correspondence as follows. As a consequence of (3.3) established in Lemma 3.1, we have

$$\frac{1}{2\pi i}\int_\Gamma \frac{f^+(y)}{y}\, dy = \alpha_0.$$

Then, from the definition of σ and the Cauchy integral formula, we obtain

$$\frac{1}{2\pi i}\int_\Gamma \frac{\sigma(y)}{y}\, dy = \frac{1}{2\pi i}\left[-\int_\Gamma \frac{2}{\alpha_1}\cdot\frac{f^+(y)}{y}\, dy + \int_\Gamma \frac{\alpha_0}{\alpha_1}\cdot\frac{1}{y}\, dy\right] = -\frac{\alpha_0}{\alpha_1}.$$

Let $\tilde{\sigma}(\zeta)$ denote

$$\tilde{\sigma}(\zeta) = \sigma(\zeta) + \frac{1}{2\pi i}\int_\Gamma \frac{\sigma(y)}{y}\, dy = -\frac{2}{\alpha_1} f^+(\zeta).$$

By normalizing $\tilde{\sigma}$ we obtain, for $\zeta \in \Gamma$,

$$f^+(\zeta) = -\frac{\tilde{\sigma}(\zeta)}{|\tilde{\sigma}(\zeta)|} \quad \text{and} \quad \theta^+(\zeta) = \arg\left(-\frac{\tilde{\sigma}(\zeta)}{|\tilde{\sigma}(\zeta)|}\right).$$

4.2. Interior Case. In this section, we describe a method to recover the interior boundary correspondence analogous to the exterior one of the previous section. We proceed by describing the solution of an integral equation corresponding to that of an exterior Laplace Dirichlet problem for a density function σ, from which the boundary correspondence may likewise be recovered by a Cauchy integral and a normalization.

Recall the Laurent series expansion for the inverted interior map

$$\frac{1}{f^-(z)} = \frac{\beta_{-1}}{z} + \beta_0 + \beta_1 z + \beta_2 z + \cdots.$$

From the case $m = 1$ of Lemma 3.2, we have that for all $z \in \Omega^+$,

$$\overline{\beta_{-1} z^{-1}} = -\frac{1}{\pi}\int_\Gamma f^-(y)\, \hat{n}\cdot\nabla_y \log|y - z| = 2\mathcal{D} f^-(z).$$

Letting z approach a boundary point $\zeta \in \Gamma$ from the exterior, and using the exterior jump relation for the double-layer potential, we obtain the integral equation

$$\overline{\beta_{-1}\zeta^{-1}} = 2\mathcal{D} f^-(\zeta) + f^-(\zeta), \quad \zeta \in \Gamma.$$

Defining the density $\tilde{\sigma}(\zeta)$ as

$$\tilde{\sigma}(\zeta) = 2(\overline{\beta_{-1}^{-1}})f^-(\zeta), \quad \zeta \in \Gamma,$$

we can rearrange the above equation to obtain the integral equation

$$\overline{\zeta^{-1}} = \left(\mathcal{D} + \frac{1}{2}\right)\tilde{\sigma}(\zeta), \quad \zeta \in \Gamma. \tag{4.2}$$

The operator $\left(D + \frac{1}{2}\right)$ has a non-trivial nullspace, which affects the solvability of this integral equation. Following [30], we remedy this by defining the operator $\mathcal{M} : C(\Gamma) \to C(\Gamma)$ as

$$\mathcal{M}\varphi = \int_\Gamma \varphi \, ds.$$

Then the following equation is uniquely solvable [30, Thm. (6.24)] for a density σ:

$$\overline{\zeta^{-1}} = \left(\mathcal{D} + \mathcal{M} + \frac{1}{2}\right)\sigma(\zeta), \quad \zeta \in \Gamma. \tag{4.3}$$

Next, we recall the following facts about the operator $\left(\mathcal{D} + \frac{1}{2}\right)$. First, the range of $\left(\mathcal{D} + \frac{1}{2}\right)$ omits the nonzero constant functions. Secondly, the null space of $\left(\mathcal{D} + \frac{1}{2}\right)$ consists of the constant functions [30, Thm. (6.21)].

If we subtract both sides of (4.3) from both sides of (4.2), we obtain that constant function $\mathcal{M}\sigma$ is in the range of the operator $\left(\mathcal{D} + \frac{1}{2}\right)$. This implies $\mathcal{M}\sigma = 0$. Thus, we find that

$$\overline{\zeta^{-1}} = \left(\mathcal{D} + \frac{1}{2}\right)\tilde{\sigma}(\zeta) = \left(\mathcal{D} + \frac{1}{2}\right)\sigma(\zeta), \quad \zeta \in \Gamma.$$

This implies $\sigma = \tilde{\sigma} + \delta$ for some $\delta \in \mathbb{C}$.

From the fact that $f^-(0) = 0$, we know that

$$\frac{1}{2\pi i}\int_\Gamma \frac{\sigma(y)}{y}\, dy = \frac{1}{2\pi i}\left[2(\overline{\beta_{-1}^{-1}})\int_\Gamma \frac{f^-(y)}{y}\, dy + \int_\Gamma \frac{\delta}{y}\, dy\right] = \delta.$$

Thus we recover $\tilde{\sigma}$ as

$$\tilde{\sigma}(\zeta) = \sigma(\zeta) - \frac{1}{2\pi i}\int_\Gamma \frac{\sigma(y)}{y}\, dy = 2(\overline{\beta_{-1}^{-1}})f^-(\zeta), \quad \zeta \in \Gamma.$$

Recalling $|f^-(\zeta)| = 1$, we normalize to find

$$f^-(\zeta) = \frac{\tilde{\sigma}(\zeta)}{|\tilde{\sigma}(\zeta)|} \quad \text{and} \quad \theta^-(\zeta) = \arg\left(\frac{\tilde{\sigma}(\zeta)}{|\tilde{\sigma}(\zeta)|}\right), \quad \zeta \in \Gamma.$$

4.3. Summary. Algorithm 4.1 captures the operational essence of the previous two sections. The algorithm is not specific to a particular choice of discretization, for which a broad range of schemes is applicable. In the next section, we provide the details for the Nyström discretization scheme with the trapezoidal rule for concreteness and for the benefit of our numerical experiments. This scheme has the advantage of being spectrally accurate, simple to implement, and amenable to acceleration.

5. Numerical Realization of the Methods. Our main concern in the numerical treatment of Algorithm 4.1 is the rapid and accurate solution of the integral equations involved.

Algorithm 4.1 Computational method for the obtaining the boundary correspondence

Require: A smooth Jordan boundary Γ, with 0 in the interior.
Require: A boundary sign s: $+1$ for exterior, -1 for interior.
Ensure: Computes the boundary correspondence θ.

STAGE 1

Solve the following integral equation for the density σ, for all $\zeta \in \Gamma$:

$$\begin{cases} \zeta = \left(\mathcal{D} - \frac{1}{2}\right)\sigma(\zeta) & \text{if } s = +1 \\ \overline{\zeta^{-1}} = \left(\mathcal{D} + \mathcal{M} + \frac{1}{2}\right)\sigma(\zeta) & \text{if } s = -1. \end{cases}$$

STAGE 2

Let $\tilde{\sigma}(\zeta) = \sigma(\zeta) + \dfrac{s}{2\pi i}\displaystyle\int_\Gamma \frac{\sigma(y)}{y}\,dy$ $(\zeta \in \Gamma)$.

STAGE 3

Let $\theta(\zeta) = \arg\left(-s\dfrac{\tilde{\sigma}(\zeta)}{|\tilde{\sigma}(\zeta)|}\right)$ $(\zeta \in \Gamma)$.

5.1. Nyström Method. We assume a boundary parametrization $\gamma : [0, L] \to \mathbb{C}$ that is $m + 2$ times continuously and periodically differentiable. The operator $\mathcal{D}$ may by substitution be evaluated in the interval $[0, L]$ using the parametric Neumann kernel ν,

$$\mathcal{D}\sigma[\gamma(x)] = \int_0^L \sigma(\gamma(y))\nu(x, y)\,dy \tag{5.1}$$

which is given by [25, p. 394]

$$\nu(x, y) = -\frac{1}{2\pi}\operatorname{Im}\begin{cases} \gamma'(y)/(\gamma(y) - \gamma(x)) & x \neq y, \\ \gamma''(x)/(2\gamma'(x)) & x = y. \end{cases}$$

We consider the discretization of this integral on an n point quadrature rule with weights $\{w_j\}_{j=1}^n$ and nodes $\{y_j\}_{j=1}^n$ on $[0, L]$, which is given by the functional $Q_n g = \sum_{j=1}^n w_j g(y_j)$. Our specific choice of quadrature rule is the *periodic trapezoidal rule*, whose weights are given by $w_j = L/n$ and the nodes are $y_j = Lj/n$, $j = 1, \ldots, n$.

The Nyström approximation $Q_n[\mathcal{D}]$ to the operator $\mathcal{D}$ uses pointwise values of the density $\mu = \sigma \circ \gamma$ at the quadrature nodes as its discrete degrees of freedom,

$$Q_n[\mathcal{D}]\mu(x) = \sum_{i=1}^n w_j \mu(y_j)\nu(x, y_j).$$

To solve the integral equation $\left(\mathcal{D} - \frac{1}{2}\right)\sigma = f$, we reduce the continuous system to the linear system in n unknowns discretized at the quadrature points

$$Q_n[\mathcal{D}]\mu_n(y_j) - \frac{1}{2}\mu_n(y_j) = f(y_j), \quad j = 1, \ldots, n. \tag{5.2}$$

Given values of a solution $\mu_n(y_1), \mu_n(y_2), \ldots, \mu_n(y_n)$ to this system, we may extend μ_n to a continuous function $\mu_n : [0, L] \to \mathbb{C}$, by way of the interpolation formula

$$\mu_n(x) = 2\left(Q_n[\mathcal{D}]\mu_n(x) - f(x)\right), \quad x \in [0, L]. \tag{5.3}$$

Then, under broadly applicable assumptions on the quadrature rule, the sequence $Q_n[\mathcal{D}]$ of operator approximations is invertible for sufficiently large $n > 0$ [30, Thm. 12.8], has uniformly bounded condition number [30, Thm. 14.3], and the sequence μ_n of approximations to the density converges uniformly as $n \to \infty$ to the solution of the continuous system [30, Cor. 12.9]. Furthermore, it can also be shown [30, Cor. 10.14] the the error in the discrete solution is bounded from above in the form $\|\mu_n - \mu\|_\infty \leq K\|(Q_n[\mathcal{D}] - \mathcal{D})\mu\|$, where K is a constant independent of n.

For an m times continuously and periodically differentiable integrand g, the trapezoidal rule admits a spectral error estimate of the form $|Q_n g - \int_0^L g\,dy| \leq Cn^{-m}\|g^{(m)}\|_\infty$, with a constant C independent of n. It follows that because of the spectral convergence of the periodic trapezoidal rule we expect spectral convergence in the number of discretization points for smooth geometries.

5.2. Fast Iterative Solution of the System. The explicit formation of the dense matrices associated with the system (5.2) may be avoided by using an iterative method such as GMRES. Using a Nyström approximation, the number of GMRES iterations for a fixed accuracy is independent of the number of unknowns [30, Sec. 14.4]. The iterative application of the operator $\mathcal{D}$ may be accelerated by considering the discrete operator $\mathcal{D}$ as the potential due to a set of sources in $\mathbb{R}^2$, and using the Fast Multipole Method (FMM [9]). Specifically, we use the potential

$$Q_n[\mathcal{D}]\sigma(y_k) = \frac{1}{2}\omega_k\kappa(y_k)\sigma(y_k) + \sum_{\substack{j=1\\ j\neq k}}^{n} \omega_j\,\hat{n}\cdot\nabla_{y_j}\log|y_j - y_k|\,\sigma(y_j), \quad k = 1,\ldots,n$$

where κ denotes the signed curvature and $\omega_j = -L/(2\pi n)\,|\gamma'(y_j)|$. On non-pathological particle distributions, the evaluation phase of the FMM runs in $O(n)$ time and the setup phase takes $O(n\log n)$ time. It follows that the overall complexity of the solve is $O(n\log n)$.

5.3. Evaluation of the Cauchy Integral. In order to recover the off-boundary values of the Riemann map, one may employ the Cauchy integral formula for the interior and exterior case (e.g. [1, Eqn. 2.6]). At target points $z \in \mathbb{C}\setminus\Gamma$ sufficiently far from the boundary, quadrature with the trapezoidal rule is sufficient to achieve high accuracy. However, numerical evaluation of Cauchy integrals presents challenges close to the boundary Γ for standard smooth quadrature rules such as the trapezoidal rule, leading to the need for an unacceptably large amount of discretization points [1]. The root cause of the challenges is the near-singularity of the integrand. A more efficient strategy for close evaluation is Quadrature by Expansion (QBX, [2, 29]), a quadrature scheme that exploits the smoothness of the potential to recover high accuracy near the boundary via appropriately placed local expansions. QBX operates by computing approximate Taylor coefficients of a potential g about centers c, so that an error estimate composed of truncation and quadrature contributions

$$\left|g(x) - \sum_{k=0}^{m}\frac{\tilde{g}^{(k)}(c)}{k!}(x-c)^k\right| \leq C_1\|\sigma\|_{C^{m+1}}r^{m+1} + C_2\left(\frac{h}{4r}\right)^{2q}\|\sigma\|_{C^{2q}}$$

can be obtained, dependent on expansion radius r, truncation order m, mesh resolution h and quadrature order q. We refer to [21] for details. QBX-based layer potential evaluation may be accelerated by ways of a fast algorithm [37, 46], with error contributions from acceleration very similar to those of conventional point-based FMMs.

TABLE 6.1

Absolute ℓ^∞ errors in the boundary correspondence on the exterior of an oval of Cassini with shape parameter α discretized with n points, computed with the methods of Section 4.3 and 5.

n	$\alpha = 5$	$\alpha = 2$	$\alpha = 1.25$	$\alpha = 1.11$	$\alpha = 1.0101$	$\alpha = 1.001001$
8	$2.38 \cdot 10^{-9}$	$2.46 \cdot 10^{-5}$	$4.43 \cdot 10^{-3}$	$2.74 \cdot 10^{-2}$		
16	$6.96 \cdot 10^{-16}$	$4.66 \cdot 10^{-9}$	$5.44 \cdot 10^{-5}$	$1.25 \cdot 10^{-3}$		
32		$6.28 \cdot 10^{-16}$	$1.15 \cdot 10^{-8}$	$4.23 \cdot 10^{-6}$	$1.57 \cdot 10^{-2}$	
64			$1.05 \cdot 10^{-15}$	$6.79 \cdot 10^{-11}$	$4.15 \cdot 10^{-4}$	$9.82 \cdot 10^{-2}$
128				$4.00 \cdot 10^{-16}$	$4.73 \cdot 10^{-7}$	$5.90 \cdot 10^{-3}$
256					$8.61 \cdot 10^{-13}$	$7.03 \cdot 10^{-5}$
512					$4.09 \cdot 10^{-16}$	$1.52 \cdot 10^{-8}$
1024						$1.11 \cdot 10^{-15}$

TABLE 6.2

Absolute ℓ^∞ errors in the boundary correspondence on the interior of an epitrochoid with shape parameter α discretized with n points, computed with the methods of Section 4.3 and 5.

n	$\alpha = 0.3$	$\alpha = 0.4$	$\alpha = 0.6$	$\alpha = 0.8$	$\alpha = 0.9$	$\alpha = 0.99$
8	$2.68 \cdot 10^{-6}$	$2.47 \cdot 10^{-5}$	$1.39 \cdot 10^{-3}$	$3.56 \cdot 10^{-2}$		
16	$2.55 \cdot 10^{-12}$	$5.38 \cdot 10^{-10}$	$1.80 \cdot 10^{-6}$	$1.24 \cdot 10^{-3}$	$2.41 \cdot 10^{-2}$	
32	$3.24 \cdot 10^{-15}$	$2.87 \cdot 10^{-15}$	$2.37 \cdot 10^{-12}$	$3.68 \cdot 10^{-7}$	$1.66 \cdot 10^{-4}$	
64			$1.44 \cdot 10^{-14}$	$5.82 \cdot 10^{-13}$	$5.84 \cdot 10^{-7}$	
128				$2.56 \cdot 10^{-14}$	$3.06 \cdot 10^{-13}$	$6.41 \cdot 10^{-3}$
256					$3.63 \cdot 10^{-14}$	$1.80 \cdot 10^{-4}$
512						$3.87 \cdot 10^{-7}$
1024						$4.66 \cdot 10^{-12}$

6. Experimental Results. We implement the method of Section 4 using the numerical approach of Section 5. In particular, our discretization is based on the periodic trapezoidal rule with the parametric Neumann kernel. We employ an FMM-accelerated GMRES solver for the solution of the integral equations based on FMMLIB [23]. The visualizations in Figures 2.1 and 6.4 were obtained using QBX for evaluation close to the curve Γ.

6.1. Smooth Domains. We test our method on a number of smooth test geometries for the interior and exterior case for which the interior or exterior boundary correspondences are available as analytical expressions. To test the accuracy of our method, we use the Nyström interpolation formula to evaluate the compute boundary correspondence at 36 points on the boundary equispaced in the parametrization variable, and report the ℓ_∞ norm of the error.

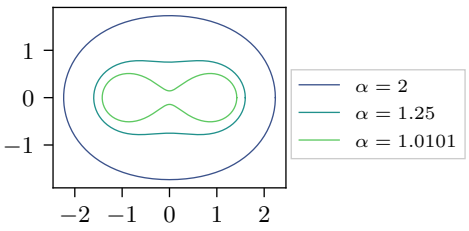

FIG. 6.1. *Oval of Cassini for various α.*

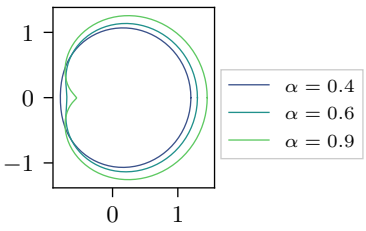

FIG. 6.2. *Epitrochoid for various α.*

6.1.1. Oval of Cassini. The oval of Cassini curve family is parametrized by $\alpha > 1$. At the limiting value $\alpha = 1$ the interior is disconnected into two components. For $\alpha \to \infty$ the domain resembles a disk of radius α. See Figure 6.1 for a visualization. The boundary parametrization and analytical value of the exterior mapping function are given by:

$$\gamma_\alpha(t) = \left(\cos(2t) + \sqrt{a^4 - \sin^2(2t)}\right)^{1/2} \exp(it), \quad t \in [0, 2\pi],$$
$$f^+(\gamma_\alpha(t)) = (\gamma_\alpha(t)^2 - 1)^{1/2}/\alpha.$$

Numerical results demonstrating the accuracy of our method for the oval of Cassini are shown in Table 6.1.

6.1.2. Epitrochoid. The epitrochoid family is parametrized by $0 \leq \alpha \leq 1$. At $\alpha = 0$ the boundary is the unit circle, while for $\alpha = 1$ the boundary is a cardioid. A subset of the tested geometries are visualized in Figure 6.2. The boundary parametrization and the analytical value of the interior mapping function are given by:

$$\gamma_\alpha(t) = \exp(it) + \frac{\alpha}{2}\exp(2it), \quad t \in [0, 2\pi],$$
$$f^-(\gamma_\alpha(t)) = \exp(it).$$

Numerical results demonstrating the accuracy of our method for the epitrochoid are shown in Table 6.2.

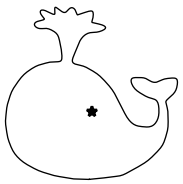

FIG. 6.3. *Whale test geometry, analytically represented as a Fourier series. The origin is marked.*

TABLE 6.3
Absolute ℓ^∞ self-convergence errors in the boundary correspondence for the 'Fourier whale' geometry discretized with n points, computed with the methods of Section 4.3 and 5.

n	Interior	Exterior
128	$7.21 \cdot 10^{-2}$	$1.07 \cdot 10^{-2}$
256	$2.29 \cdot 10^{-3}$	$4.16 \cdot 10^{-4}$
512	$1.24 \cdot 10^{-5}$	$3.61 \cdot 10^{-6}$
1024	$8.10 \cdot 10^{-10}$	$7.90 \cdot 10^{-11}$
2048	$2.77 \cdot 10^{-12}$	$4.07 \cdot 10^{-13}$
4096	$2.80 \cdot 10^{-12}$	$4.11 \cdot 10^{-13}$

6.1.3. Fourier Whale. We also report the results for a complicated smooth geometry for which the boundary correspondence is not analytically available. The geometry in Figure 6.3, with the origin marked, was obtained by parametrizing the boundary of the image of a spouting whale from the EmojiOne project [20]. Specifically, we used a parametrization $\gamma(t) = \gamma_1(t) + i\gamma_2(t), t \in [0, 2\pi]$, such that the functions γ_1 and γ_2 are given by 53-term Fourier interpolants of selected boundary points. Since the boundary correspondence is not analytically available, we test the accuracy using a self-convergence test. We solve for the boundary correspondence using 2^{13} discretization points. Using this value as a reference solution, we estimate the accuracy for a given number of discretization points by comparing values at 36 points equispaced in the parameter domain. We report the absolute ℓ^∞ error for different discretization point counts in Table 6.3. The Riemann maps we found for this geometry are visualized in Figure 6.4.

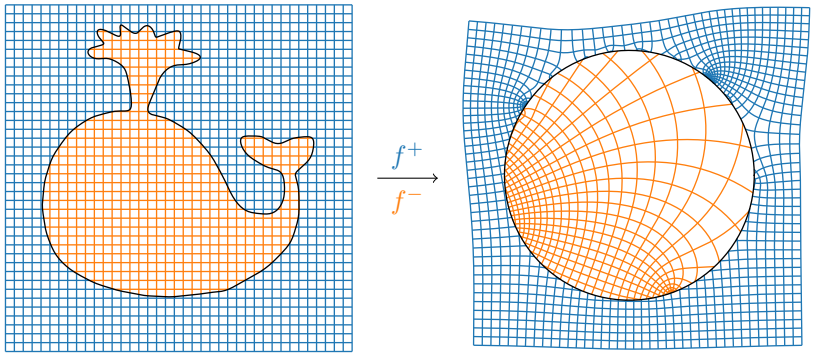

FIG. 6.4. *Graphical representation of the Riemann maps for the interior/exterior of the whale domain.*

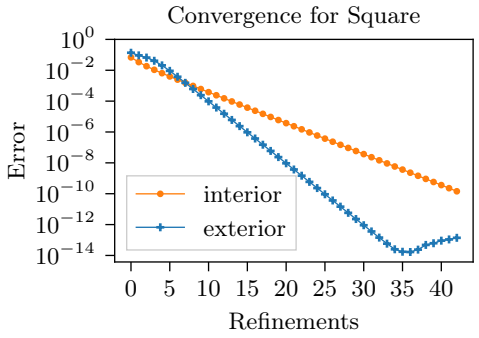

FIG. 6.5. *Estimated absolute ℓ^∞ errors for the unit square with increasing refinement. The initial system size was* 36 *unknowns and each refinement added* 72 *unknowns, up to* 3060 *unknowns.*

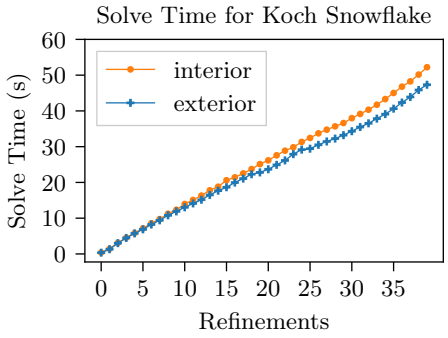

FIG. 6.6. *Solve time for system associated with the Koch snowflake using an FMM-accelerated GMRES solver. The initial system size was* 1728 *unknowns and each refinement added* 3456 *unknowns, up to* 136512 *unknowns.*

6.1.4. Discussion: Accuracy on Smooth Geometries. It is evident from these results that our methods, combined with a Nyström/trapezoidal scheme, exhibit spectral convergence. The examples in this section have been used in previous research to test the accuracy of integral equation methods for obtaining the boundary correspondence; for instance, for analogous experiments using the Nyström method applied to the Kerzman-Stein integral equation, see [44] for the interior case and [33] for the exterior case. We find that these results have a similar level of accuracy to the results for the Nyström solution of integral equations based on the Kerzman-Stein kernel. In the next section, we will apply our method to a domain with a corner, for which the trapezoidal rule is not an ideal quadrature method.

6.2. Domains with Corners. It is well known that the Nyström method with the trapezoidal rule does not retain its high order accuracy on boundaries with corners, due to the presence of singularities in the integral kernel at the corner. Nevertheless, a high accuracy solution can be recovered with modifications to the scheme. We review one of these techniques and give numerical results in the case of the square.

The technique we use is based on a simplified version of the quadrature technique

described in [6]. We use composite Gauss-Legendre panels refined dyadically towards the corners of the square. The last two panels on either side of each corner are omitted. Additionally, each unknown is multiplied by the square root of the quadrature weight as a way to improve conditioning (see [6] for details).

For the reference solution, we compute the boundary correspondence at 36 equispaced points on the unit square. We use the SC Toolbox [14] to compute the Schwarz-Christoffel map from the disk to the square, and then we invert this map with the provided `evalinv` subroutine.

The experimental results on the accuracy of our method are given in Figure 6.5. The results show the absolute ℓ^∞ error in the boundary correspondence versus the number of refinements that were made recursively to the panels closest to the corner points. The Gauss-Legendre panels had 9 points per panel. Starting with one panel per side, each refinement added two panels per side half the width of the previous near-corner panels.

This scheme is able to recover up to 13–14 digits of accuracy in the exterior case and 10 digits in the interior case. The difference in convergence speeds between the interior and the exterior of the square is the subject of future investigation. We have chosen this scheme for its simplicity, though more advanced schemes can both improve the accuracy and reduce the number of unknowns required.

6.3. Scaling. To study the scaling of our method, we time our implementation of the solve phase of Algorithm 4.1, which is the dominant contribution to the cost of the algorithm. The test geometry is the fourth iteration of a Koch snowflake curve, which has 192 corners (see Figure 2.1 for a visualization) and the system contains up to 136512 unknowns. We use the quadrature scheme described in Section 6.2 and measure the wall time of the algorithm with increasing refinements. The timing results, obtained on a single core of a dual-socket 2.2 GHz Intel Xeon E5-2650 v4 processor, are presented in Figure 6.6. After 39 refinements, the mapping obtains approximately 7–8 digits of accuracy according to direct comparison with results from the SC Toolbox. As expected, the timing data demonstrates the solve phase of the algorithm scales close to linearly with the number of unknowns.

7. Conclusions. This paper makes two contributions.

First, we characterize the density functions σ that give rise to harmonic polynomials represented as double-layer potentials $\mathcal{D}\sigma$ on the interior of a piecewise smooth Jordan domain, and their counterparts that give rise to Laurent polynomials on the exterior of the domain. We show how these density functions relate to the Riemann maps associated with the domain. In addition to the described application to conformal mapping, this work may be of mathematical interest for those studying the behavior of the double-layer potential and numerical methods for it.

Second, we derive an integral equation whose solution allows us to recover the boundary correspondence for the exterior or interior mapping function. From a practical standpoint, our equation is second-kind, uniquely solvable and has a continuous kernel, which leads to a robust and simple discretization with the Nyström method. We further demonstrate the effective acceleration of the method, avoiding quadratic complexity in all parts of the method. A major advantage of the double-layer potential is the ready availability of existing fast solvers, such as those in [5, 7, 26, 37, 39]. Our experiments demonstrate that the method achieves spectral accuracy on smooth domains, with results of comparable accuracy to those based on the solution of integral equations using the Kerzman-Stein kernel. Finally, we demonstrate that the method can be made accurate in the presence of corners.

Acknowledgments. The authors' research was supported by the National Science Foundation under grants DMS-1418961 and DMS-1654756. Part of the work was performed while the authors were participating in the HKUST-ICERM workshop 'Integral Equation Methods, Fast Algorithms and Their Applications to Fluid Dynamics and Materials Science' held in 2017. The authors would also like to thank the anonymous reviewers whose comments have helped to improve the manuscript.

REFERENCES

[1] A. Barnett, B. Wu, and S. Veerapaneni, *Spectrally accurate quadratures for evaluation of layer potentials close to the boundary for the 2D Stokes and Laplace equations*, SIAM J. Sci. Comput., 37 (2015), pp. B519–B542.

[2] A. H. Barnett, *Evaluation of layer potentials close to the boundary for Laplace and Helmholtz problems on analytic planar domains*, SIAM J. Sci. Comput., 36 (2014), pp. A427–A451.

[3] J.-P. Berrut, *A Fredholm integral equation of the second kind for conformal mapping*, J. Comput. Appl. Math., 14 (1986), pp. 99–110. Special issue on numerical conformal mapping.

[4] G. Birkhoff, *The Numerical Solution of Elliptic Equations*, Society for Industrial and Applied Mathematics, 1972.

[5] J. Bremer, *A fast direct solver for the integral equations of scattering theory on planar curves with corners*, J. Comput. Phys., 231 (2012), pp. 1879–1899.

[6] ———, *On the Nyström discretization of integral equations on planar curves with corners*, Applied and Computational Harmonic Analysis, 32 (2012), pp. 45 – 64.

[7] J. Bremer, A. Gillman, and P.-G. Martinsson, *A high-order accurate accelerated direct solver for acoustic scattering from surfaces*, BIT, 55 (2015), pp. 367–397.

[8] G. Carrier, M. Krook, and C. Pearson, *Functions of a Complex Variable: Theory and Technique*, Society for Industrial and Applied Mathematics, 2005.

[9] J. Carrier, L. Greengard, and V. Rokhlin, *A fast adaptive multipole algorithm for particle simulations*, SIAM Journal on Scientific and Statistical Computing, 9 (1988), pp. 669–686.

[10] J. B. Conway, *Functions of One Complex Variable I*, Springer Science & Business Media, Aug. 1978. Google-Books-ID: 9LtfZr1snG0C.

[11] J. H. Curtiss, *Faber polynomials and the Faber series*, Amer. Math. Monthly, 78 (1971), pp. 577–596.

[12] T. K. DeLillo and A. R. Elcrat, *A comparison of some numerical conformal mapping methods for exterior regions*, SIAM J. Sci. Statist. Comput., 12 (1991), pp. 399–422.

[13] ———, *Numerical conformal mapping methods for exterior regions with corners*, J. Comput. Phys., 108 (1993), pp. 199–208.

[14] T. A. Driscoll, *Schwarz–Christoffel Toolbox User's Guide*, 2.3 ed.

[15] T. A. Driscoll, K.-C. Toh, and L. N. Trefethen, *From potential theory to matrix iterations in six steps*, SIAM Rev., 40 (1998), pp. 547–578.

[16] M. Eiermann, *On semiiterative methods generated by Faber polynomials*, Numer. Math., 56 (1989), pp. 139–156.

[17] S. W. Ellacott, *Computation of Faber series with application to numerical polynomial approximation in the complex plane*, Math. Comp., 40 (1983), pp. 575–587.

[18] ———, *On the Faber transform and efficient numerical rational approximation*, SIAM J. Numer. Anal., 20 (1983), pp. 989–1000.

[19] ———, *A survey of Faber methods in numerical approximation*, Comput. Math. Appl. Part B, 12 (1986), pp. 1103–1107.

[20] EmojiOne authors. https://github.com/emojione/emojione, 2017. v2.2.7 tag; retrieved 2018-02-21.

[21] C. L. Epstein, L. Greengard, and A. Klöckner, *On the convergence of local expansions of layer potentials*, SIAM J. Numer. Anal., 51 (2013), pp. 2660–2679.

[22] D. Gaier, *Konstruktive Methoden der konformen Abbildung*, Springer Tracts in Natural Philosophy, Vol. 3, Springer-Verlag, Berlin, 1964.

[23] Z. Gimbutas and L. Greengard, *FMMLIB2D*. https://github.com/zgimbutas/fmmlib2d. v1.2.1 tag; retrieved 2018-06.

[24] M. H. Gutknecht, *Numerical conformal mapping methods based on function conjugation*, J. Comput. Appl. Math., 14 (1986), pp. 31–77. Special issue on numerical conformal mapping.

[25] P. Henrici, *Applied and computational complex analysis. Vol. 3*, Pure and Applied Mathematics (New York), John Wiley & Sons, Inc., New York, 1986. Discrete Fourier analysis—Cauchy

integrals—construction of conformal maps—univalent functions, A Wiley-Interscience Publication.

[26] K. L. Ho and L. Greengard, *A fast direct solver for structured linear systems by recursive skeletonization*, SIAM J. Sci. Comput., 34 (2012), pp. A2507–A2532.

[27] L. V. Kantorovich and V. I. Krylov, *Approximate methods of higher analysis*, Translated from the 3rd Russian edition by C. D. Benster, Interscience Publishers, Inc., New York; P. Noordhoff Ltd., Groningen, 1958.

[28] N. Kerzman and M. R. Trummer, *Numerical conformal mapping via the Szegő kernel*, J. Comput. Appl. Math., 14 (1986), pp. 111–123. Special issue on numerical conformal mapping.

[29] A. Klöckner, A. Barnett, L. Greengard, and M. O'Neil, *Quadrature by expansion: a new method for the evaluation of layer potentials*, J. Comput. Phys., 252 (2013), pp. 332–349.

[30] R. Kress, *Linear integral equations*, vol. 82 of Applied Mathematical Sciences, Springer, New York, third ed., 2014.

[31] U. Leonhardt, *Optical conformal mapping*, Science, 312 (2006), pp. 1777–1780.

[32] I. Moret and P. Novati, *An interpolatory approximation of the matrix exponential based on Faber polynomials*, J. Comput. Appl. Math., 131 (2001), pp. 361–380.

[33] A. Murid, M. Nashed, M. Razali, et al., *Numerical conformal mapping for exterior regions via the Kerzman–Stein kernel*, J. Integral Equ. Appl., 10 (1998), pp. 517–532.

[34] E. Nyström, *Über Die Praktische Auflösung von Integralgleichungen mit Anwendungen auf Randwertaufgaben*, Acta Mathematica, 54 (1930), pp. 185–204.

[35] S. T. O'Donnell and V. Rokhlin, *A fast algorithm for the numerical evaluation of conformal mappings*, SIAM J. Sci. Statist. Comput., 10 (1989), pp. 475–487.

[36] C. Pommerenke, *Boundary behaviour of conformal maps*, vol. 299 of Grundlehren der Mathematischen Wissenschaften [Fundamental Principles of Mathematical Sciences], Springer-Verlag, Berlin, 1992.

[37] M. Rachh, A. Klöckner, and M. O'Neil, *Fast algorithms for Quadrature by Expansion I: Globally valid expansions*, J. Comput. Phys., 345 (2017), pp. 706–731.

[38] Y. Saad and M. H. Schultz, *GMRES: A Generalized Minimal Residual Algorithm for Solving Nonsymmetric Linear Systems*, SIAM Journal on Scientific and Statistical Computing, 7 (1986), pp. 856–869.

[39] W. Śmigaj, T. Betcke, S. Arridge, J. Phillips, and M. Schweiger, *Solving boundary integral problems with BEM++*, ACM Trans. Math. Software, 41 (2015), pp. Art. 6, 40.

[40] G. Starke and R. S. Varga, *A hybrid Arnoldi-Faber iterative method for nonsymmetric systems of linear equations*, Numer. Math., 64 (1993), pp. 213–240.

[41] P. K. Suetin, *Series of Faber polynomials*, vol. 1 of Analytical Methods and Special Functions, Gordon and Breach Science Publishers, Amsterdam, 1998. Translated from the 1984 Russian original by E. V. Pankratiev.

[42] G. T. Symm, *An integral equation method in conformal mapping*, Numer. Math., 9 (1966), pp. 250–258.

[43] G. T. Symm, *Numerical mapping of exterior domains*, Numerische Mathematik, 10 (1967), pp. 437–445.

[44] M. R. Trummer, *An efficient implementation of a conformal mapping method based on the Szegö kernel*, SIAM J. Numer. Anal., 23 (1986), pp. 853–872.

[45] G. Tsamasphyros and A. Giannakopoulos, *Automatic optimum mesh around singularities using conformal mapping*, Engineering Fracture Mechanics, 23 (1986), pp. 507 – 520.

[46] M. Wala and A. Klöckner, *A fast algorithm with error bounds for quadrature by expansion*, Journal of Computational Physics, 374 (2018), pp. 135 – 162.

[47] S. E. Warschawski, *Recent results in numerical methods of conformal mapping*, in Proceedings of Symposia in Applied Mathematics. Vol. VI. Numerical analysis, McGraw-Hill Book Company, Inc., New York, for the American Mathematical Society, Providence, R. I., 1956, pp. 219–250.

[48] R. Wegmann, *Methods for numerical conformal mapping: dedicated to the memory of Dieter Gaier*, in Geometric function theory, Elsevier, 2005, pp. 351–477.